Published in final edited form as:
Magn Reson Med. 2007 July ; 58(1): 70–81. doi:10.1002/mrm.21255.

Perfusion Mapping With Multiecho Multishot Parallel Imaging EPI

Rexford D. Newbould[1,*], **Stefan T. Skare**[1], **Thies H. Jochimsen**[3], **Marcus T. Alley**[1], **Michael E. Moseley**[1], **Gregory W. Albers**[2], and **Roland Bammer**[1]

[1]Lucas MRS/I Center, Department of Radiology, Stanford University, Stanford, California, USA.

[2]Stanford Stroke Center, Department of Neurology, Stanford University, Stanford, California, USA.

[3]Max Planck Institute for Human Cognitive and Brain Sciences, Leipzig, Germany.

Abstract

Echo-planar imaging (EPI) is the standard technique for dynamic susceptibility-contrast (DSC) perfusion MRI. However, EPI suffers from well-known geometric distortions, which can be reduced by increasing the *k*-space phase velocity. Moreover, the long echo times (TEs) used in DSC lead to signal saturation of the arterial input signal, and hence to severe quantitation errors in the hemodynamic information. Here, through the use of interleaved shot acquisition and parallel imaging (PI), rapid volumetric EPI is performed using pseudo-single-shot (ss)EPI with the effective T_2^* blur and susceptibility distortions of a multishot EPI sequence. The reduced readout lengths permit multiple echoes to be acquired with temporal resolution and spatial coverage similar to those obtained with a single-echo method. Multiecho readouts allow for unbiased R_2^* mapping to avoid incorrect estimation of tracer concentration due to signal saturation or T_1 shortening effects. Multiecho perfusion measurement also mitigates the signal-to-noise ratio (SNR) reduction that results from utilizing PI. Results from both volunteers and clinical stroke patients are presented. This acquisition scheme can aid most rapid time-series acquisitions. The use of this method for DSC addresses the problem of signal saturation and T_1 contamination while it improves image quality, and is a logical step toward better quantitative MR PWI.

Keywords

perfusion; dynamic susceptibility contrast; bolus tracking; parallel imaging

Dynamic susceptibility contrast (DSC)-based perfusion-weighted imaging (PWI) can visualize cerebrovascular hemodynamics. Therefore, it may be an important asset to determine “tissue-at-risk” in acute stroke patients. When used with diffusion-weighted imaging (DWI), it can help to triage patients who would potentially benefit from IV tPA treatment or mechanical thrombectomy (1). In DSC imaging, an exogenous paramagnetic

[*]Correspondence to: Rexford D. Newbould, Lucas MRS/I Center, 1201 Welch Rd., Mail Code 5488, Room PS-055, Stanford, CA 94305-5488. newbould@stanford.edu.

tracer (e.g., Gd-DTPA or Dy-DTPA) is rapidly injected into the venous system and its passage is tracked through concentration-related T_2^* changes in the cerebral vascular bed (2–4). The arterial input concentration curve, as measured in a large cranial vessel, defines the arterial input function (AIF) (5), which is necessary to define the arrival and non-ideal shape of the impulse bolus injection as it reaches the imaging volume. The undesired temporal smearing of the concentration curve is undone via deconvolving the AIF from the signal course. This leaves the tissue residue function, which can be used to infer important information about the hemodynamic state of the tissue, such as the cerebral blood volume (CBV), cerebral blood flow (CBF), and mean transit time (MTT).

In order to sufficiently track the first-pass contrast concentration changes, which typically occur over a time span of approximately 10 s, rapid time-series imaging is required. This has made single-shot echo-planar imaging (ssEPI) (6) the method of choice for most DSC perfusion imaging. However, the use of ssEPI suffers from several well-known problems, some of which are exacerbated in DSC imaging.

The T_2^* decay of the signal during the EPI readout widens the sampling's point-spread function (PSF), blurring the output images and effectively limiting resolution (7,8). Further, due to the T_2^* decay, the signal exists for only a short period of time, which places an absolute upper limit on the possible resolution. The introduction of the tracer greatly decreases T_2^*, generating significant vessel blooming during the bolus passage due to the larger susceptibility gradients. This resolution decay is most notable cortically, as a result of the venous drainage of the agent, and near the major cranial arteries, leading to an apparent widening of vessels.

EPI suffers from well-described geometric image distortions due to the low sampling bandwidth in the phase-encoding direction. Aside from global distortions, local areas of magnetic field susceptibility gradients (e.g., near the sinuses and the auditory canals), which are most egregious at air/tissue interfaces, suffer from image voids, with signal energy "piled-up" nearby. For DSC PWI this is highly problematic since the signal from the carotid siphon or the inferior cerebral arteries in the sella region, such as the internal carotid artery (ICA) and middle cerebral artery (MCA), are commonly used to define the AIF. These areas are often markedly distorted due to the strong susceptibility gradients.

Due to the relatively long TEs needed for optimal T_2^* contrast in brain parenchyma, the contrast material in the arteries during bolus passage can so greatly reduce T_2^* that the contribution from the additive, rectified noise floor is comparable to the Rician-distributed MR magnitude signal. This leads to an underestimation of the tracer concentration curves (9). During bolus passage, the difference in susceptibility between the tissue and the paramagnetic material in the large arterial vessels causes significant local resonance frequency shifts. Combined with EPI's low pixel bandwidth in the phase-encoding direction, significant shifts of the vessel can be observed, causing degradation of the AIF curve shape. These image-quality issues associated with EPI can preclude accurate determination of the AIF, affecting the veracity of the measured CBV, MTT, and CBF.

In this work an interleaved EPI acquisition with parallel imaging (PI) reconstruction is used to overcome both the image-quality and contrast-mapping drawbacks found in ssEPI. Through PI, the temporal resolution of the interleaved EPI acquisitions can be accelerated above that of ssEPI, with the added benefit of acquiring multiple echoes of each slice in each volume. Since the reduced readout lengths of PI-enhanced EPI scans allow multiple echoes to be acquired without a penalty in time resolution, unbiased R_2^* mapping is possible. This avoids incorrect estimation of tracer concentration due to signal saturation or T_1-shortening effects. It can be anticipated that rapid volumetric EPI for DSC can be performed using this pseudo-ssEPI acquisition, with the effective T_2^* blur and susceptibility distortions being reduced to the magnitude of a multiple-interleaf EPI sequence. Improved image quality, combined with the additional echo information, results in improved DSC mapping of the hemodynamic parameters.

THEORY

A decrease in image distortion can be expected when the *k*-space sampling velocity, dk_y/dt(and thus the bandwidth per pixel), is increased in the phase-encoding direction (10), such as by acquiring the *k*-space over several excitation experiments in an interleaved fashion. An *M*-interleaved EPI acquisition samples $1/M^{\text{th}}$ of the phase-encoding lines in each shot, and thus *k*-space will be traversed *M*-times faster and the phase accrual from off-resonant spins during the course of the EPI readout will diminish by *M*. However, interleaved EPI reduces some of the advantages of using ssEPI, such as its great tolerance to patient motion and ability to form images rapidly. An interleaved EPI acquisition with *M*shots takes *M* × TR to acquire a single image, which reduces the net temporal resolution. Methods that require a temporal resolution of 1–2 s to characterize the AIF, such as bolus-tracking perfusion, have met with limited success when conventional interleaved EPI is used. Furthermore, rapid contrast changes occur during the bolus passage. These intensity variations between interleaves can cause ghosting artifacts. Interleaved EPI with DSC can be achieved by using very short TRs; however, the reduced baseline signal and the increased sensitivity to T_1 changes during the bolus passage and the tracer retention may impair the calculation of tracer concentration from R_2^* changes.

Similarly to interleaved EPI, the reduced number of phase-encoding steps needed in PI also increases the phase-direction *k*-space sampling velocity and thus reduces susceptibility and blurring artifacts. The reduction in blurring and distortions (11) and resolution enhancement (12) obtained with PI-EPI have been explored previously by a number of authors. Given that both PI-EPI and interleaved EPI acquisitions acquire a reduced *k*-space in an identical manner, their combination is a natural result (Fig. 1). A time-series of data, such as in DSC-PWI, may be acquired using interleaved EPI. However, the time resolution of interleaved EPI is unsuitable for resolving the passage of the contrast material. Nevertheless, by means of PI every interleaf can be reconstructed separately, maintaining the same temporal resolution as ssEPI. In addition to restoring the temporal resolution, the data acquired in such a fashion retain the increased resolution and reduced T_2^* blur and susceptibility distortions of interleaved EPI due to the faster *k*-space traversal. As every *M*acquisitions form a complete *k*-space, this dataset may be used for an autocalibrating PI method (Fig. 1).

Another distinct advantage to the reduced readout length with a multishot/PI-EPI method is that it allows the acquisition of multiple echoes while maintaining whole-brain coverage and a near 1-s temporal resolution. This comes without penalty as the shorter readout train with an identical TE introduces a gap between excitation and reception, which can be used to acquire the additional echoes. The benefit of multiple echoes in PWI was shown to be beneficial by Vonken et al. (13,14), who proposed the use of a second, earlier echo with reduced signal saturation effects, leading to reduced error in the computed arterial input concentration and the derived hemodynamic metrics. In their studies, the first TE was used for the AIF measurement and the second TE was used for the measurement of the contrast passage through the tissue. Since the underlying T_2^* varies, especially during the tracer passage, the optimum TE is also variable. In this work we were able to acquire up to four echoes due to the *M*times shorter readout train.

Multiecho DSC allows the calculation of true R_2^* maps for each volume without any influence from T_1 relaxation, rather than relying on the relative signal difference from a prebolus baseline measurement as a ΔR_2^* analogue. This is of increased relevance for higher temporal resolutions (or decreased TRs) as the T_1 effect of the contrast agent (CA) counteracts the T_2^* effect. Decreased TRs with equal coverage are also possible with the shorter readouts of this method, as the sequence time after the last effective time is shortened *M*times. Previous multiecho methods used only two echoes due to time constraints (i.e., much longer readout lengths per EPI train) (13,14), which reduced the ability to perform accurate R_2^* mapping. Signal voids in the later of the two echoes would confound dual-echo methods, thus underestimating R_2^* and the tracer concentration (9). When using PI with multiecho DSC, several echoes may be acquired in a similar amount of time as that of a single echo in an ssEPI method. Later echoes may be removed from the fit as needed or selectively weighted based on voxel signal level without removing the ability to calculate R_2^*. Finally, as multiecho DSC does not rely on a prebolus baseline image, it is less sensitive to any bulk motion between the start and completion of scanning.

The combination of multiecho interleaved EPI with PI for restoration of temporal resolution was implemented and tested clinically, and is referred to as PERfusion with Multiple Echoes and Temporal Enhancement (PERMEATE) (15). In PERMEATE, multiple echoes of a volume are read out and split up among each of the several interleaves (Fig. 1). Hybrid-space generalized autocalibrating partially parallel acquisitions (GRAPPA) (16) PI calibration is performed by combining the first *M* prebolus interleaves to form a fully sampled *k*-space. Each shot is then reconstructed separately using these determined GRAPPA-like weights, forming a quasi-single-shot dataset with a temporal resolution of 1 TR, and the effective distortions and blurring of an *M*-shot interleaved EPI acquisition. During each TR the echoes per slice obtained allow calculation of R_2^* on a per-pixel basis by means of a magnitude-weighted nonlinear fit. Finally, slice acquisition is interleaved throughout the TR. The total number of slices acquired per TR is determined by the EPI readout duration (i.e., number of interleaves), number of echoes desired, and TR. In practice, a near 1-s temporal resolution could be obtained with 15 slices over three or four interleaves and three or four echoes.

MATERIALS AND METHODS

A multishot, multiecho, multislice gradient-echo (GRE) EPI pulse sequence was developed and implemented on a GE Signa Excite platform (GE Healthcare, Waukesha, WI; 40 mT/m, SR = 150 mT/m/s) at 1.5T. The free induction decay (FID) following a spectral-spatial excitation was read out by several interleaved EPI readout trains, where each readout train acquired the same $1/M^{th}$ of a 96 × 96 *k*-space, as shown in Fig. 1. Readout trains were placed as densely as allowed by system limitations, with the final readout TE no later than 60 ms. Slice acquisition was interleaved throughout the TR. The true acquisition time of each slice was tagged for the subsequent time-series analysis. The multiple GRE readout EPI sequence is illustrated in Fig. 2. Fifteen 5-mm slices with a 1.5-mm gap were acquired per TR using either an eight-channel phased-array head coil (Invivo, Peewaukee, WI, USA) or an eight-channel neurovascular phased-array coil operated in the head-only mode (Invivo, Peewaukee, WI, USA). For both coils the built-in quadrature body coil was used for signal excitation. The response from the first two excitations of the dynamic series was discarded to avoid confounding effects from the signal as it transitioned into steady state. A single-dose bolus injection (0.1 mM/kg of Gd-DTPA, Omniscan; GE Healthcare, Chalfont St. Giles, UK) was performed at a rate of 4 ml/s 15 s into the scan using a dual-piston power injector (Spectris, Medrad, Indianola, PA, USA), followed immediately by a 20-ml saline flush. Imaging was done on three normal volunteers and 44 patients who had been admitted for stroke-like presentation. Informed consent was obtained from all scan subjects, and all protocols were approved by the institution's review board.

Two versions of PERMEATE as well as one standard version of GRE-ssEPI were used for clinical PWI, and all required an identical scan time of 1 min 14 s. Specifically, the first PERMEATE version, a three-interleaf, three-echo version (TE = 14.6 ms, 33.8 ms, and 53.0 ms, TR = 1.225 s), acquired 20 volumes (including discarded acquisitions), resulting in a total of 60 volumes after PI reconstruction. The second PERMEATE version, a four-interleaf, four-echo version (TE = 12.4 ms, 27.4 ms, 42.4 ms, and 57.4 ms, TR = 1.225 s), acquired 15 volumes in the same scan time, leading again to 60 volumes after the final PI reconstruction. For comparative evaluation, GRE-ssEPI was acquired instead of a PERMEATE acquisition for randomly selected patients (TE = 60 ms, TR = 2.0 s), with 36 volumes acquired in the same scan time. Due to the longer EPI readout, a longer TR of 2 s was required to afford whole-brain coverage. The effect of different TRs will be addressed in subsequent sections.

In the four-interleaf PERMEATE acquisition, the otherwise sequential shot ordering was altered. Here the shot order was permuted to a 1,3,2,4 order instead of a 1,2,3,4 order. When this ordering is used, every sequential pair of shots (e.g., 1 and 3, 2 and 4, etc.) may be combined to form a *k*-space that uses an $R = 2$ acquisition pattern. The use of this ordering does not change the PI reconstruction for the $R = 4$ case. The $R = 2$ reconstruction allows an increased SNR though decreased temporal resolution that is between the high-temporal-resolution $R = 4$ and classic, high-SNR $R = 1$ reconstructions. When a short TR is used, this $R = 2$ reconstruction may offer a trade-off between SNR and temporal resolution, without T_1 bias. This shot ordering is illustrated in Fig. 1.

Automatic correction (17) of Nyquist ghosts resulting from odd/even echo misalignment was used to eliminate the reference prescan, which on the systems used can take a substantial amount of additional scan time for interleaved EPI approaches. Hybrid-space (i.e., *x*-k_y space) PI reconstruction (16) was used to restore temporal resolution for the PERMEATE image data sets, in which each interleaf was restored to a full-FOV image. The result was 60 multiecho volumes with a temporal resolution of 1.225 s for both the three- and four-shot versions. For each slice, GRAPPA-like weights were calculated using every interleave of the first echo in the first nondiscarded imaging time point and then applied to all echoes and time samples in the PERMEATE dynamic series. The first *R*shots of the dynamic series were discarded to avoid artifacts from transitioning into steady state. Automatic image-based in-plane motion correction was then performed on the first echo of each volume by minimizing the sum-of-squares (SoS) difference between images (18). Motion correction parameters determined from this first echo were then applied to every echo in the volume.

R_2^* maps were calculated from the PERMEATE image sets by calculating R_2^* in each voxel in every volume using a weighted SoS minimization fit to the well-known signal equation for decay with increasing TE:

$$I(TE)=S_{app}\cdot e^{-TE\cdot R_2^*} \quad [1]$$

where the apparent equilibrium signal magnitude, S_{app}, contains both proton density and T_1 contributions. A baseline R_2^* was calculated by averaging all R_2^* maps from the prebolus volumes. This baseline $R_2^*(R_{2bline}^*)$ was then subtracted from every R_2^* map so that the prebolus R_2^* was approximately zero in order to aid comparison with the single-echo ΔR_2^* maps. That is, the ΔR_2^* of the fitted multiecho datasets is calculated as:

$$\Delta\, R_2^*(t) \equiv R_2^*(t) - R_{2,bline}^* \quad [2]$$

In addition, ΔR_2^* maps were calculated from the single-echo data using:

$$\Delta\, R_2^*(t) \equiv (R_2^*(t)-R_{2,bline}^*)=-\frac{1}{TE}\cdot\ln\left(\frac{I(t)(1-e^{-TR/T_{1,bline}})}{I_{bline}(1-e^{-TR/T_1(t)})}\right),\left[\begin{array}{c} assuming \\ T_{1,bline}=T_1(t)\end{array}\right]\Rightarrow \Delta\,\tilde{R}_2^*(t)=-\frac{1}{TE}\cdot\ln\left(\frac{I(t)}{I_{bline}}\right) \quad [3]$$

where $I(t)$ is the current image intensity, and $I_{bline}$is the prebolus, baseline image intensity. This baseline intensity was calculated using the time average intensity of the prebolus images. It is important to note that $S_{app}$from Eq. [1] is the apparent proton density, which includes T_1 effects, removing them for each point in time from the R_2^* calculation. Equation [3] uses the current image intensity I_0, and it assumes that T_1 is static throughout the time series. T_1 effects from presence of the tracer material thus bias the ΔR_2^* calculation.

Perfusion parameters were calculated using the resulting ΔR_2^* time courses on a pixel-by-pixel basis. Automatic AIF identification of candidate voxels (19) using cluster analysis with timing and anatomical considerations was performed on the time-course volumes to identify

40 AIF voxels, which were then combined. The AIFs ΔR_2^* values (ms^{-1}) were converted to CA concentration (mM) in the blood, $[CA]_{blood}$, using the bulk blood relaxivity at 1.5T (20):

$$[\mathrm{CA}]_{\mathrm{blood}} = -6.646 + \sqrt{44.174 + 1742.2 \cdot \Delta R_2^*} \quad [4]$$

The tissue residue function ($\boldsymbol{R} = [R(T_1), R(T_2), \ldots, R(t_N)]^T$) was computed on a per-pixel basis using a block-circulant singular-value (SV) decomposition-based, Tikhonov-regularized ($SV_{thresh} = 0.2 \times SV_{max}$) deconvolution of the automatically identified AIF from the tissue CA concentration time response pixel by pixel. That is, $\boldsymbol{R} = \mathbf{A}^{-1}\,\mathbf{c}_T$ was formulated as $\boldsymbol{R} = \mathbf{V}\,\mathrm{diag}(1/\mathbf{SV})\mathbf{U}^T\,\mathbf{c}_T$. Here, **A** is the block-circulant formulation of the AIF ($\mathbf{A_1} = [AIF(T_1), AIF(T_2), \ldots AIF(t_N)]^T$, $\mathbf{A_2} = [AIF(t_N), AIF(T_1), \ldots AIF(t_{N-1})]^T$, … $\mathbf{A_N} = [AIF(T_2), AIF(t_3), \ldots AIF(T_1)]^T$ and $\mathbf{A} = [\mathbf{A}_1, \mathbf{A}_2, \ldots \mathbf{A}_N]$), and the tissue concentration $\mathbf{c}_T = [C_T(T_1), C_T(T_2), \ldots, C_T(t_N)]^T$, where $C_T(t)$ is the R_2^*-proportional tissue tracer concentration. The tracer concentration in tissue (mM) was calculated from the tissue's ΔR_2^* (ms^{-1}) using $[CA]_{tissue} = 22.7273 \cdot \Delta R_2^*$ (21). It has been shown that the block-circulant SV deconvolution is less sensitive to tracer arrival timing than the regular SV deconvolution (22).

Using the AIF, the tissue tracer concentration C_T, and the calculated tissue residue function $R(t)$, the resultant CBV, CBF, and MTT maps were calculated using the following formulas:

$$CBV = \frac{k_h \int_{-\infty}^{\infty} C_T(\tau)\,d\tau}{\int_{-\infty}^{\infty} AIF(\tau)\,d\tau} \quad [5]$$

$$MTT \equiv \frac{\int_{-\infty}^{\infty} R(\tau)\,d\tau}{\max(R(t))} \quad [6]$$

$$CBF \equiv \frac{CBV}{MTT} \quad [7]$$

where $R(t)$ is the deconvolved tissue residue function (23,24). The values were also corrected for differences between large- and small-vessel hematocrits using a $k_h = (1–0.45)/(1–0.25)/1.04$ (3).

For comparative evaluation, each echo from the PERMEATE acquisition was also separated into its own single-echo dataset, and ΔR_2^* estimation used the same metrics (Eq. [3]) as the single-echo GRE-ssEPI data. Perfusion calculations were then performed on each new ΔR_2^* dataset. These new datasets allow comparison of the benefits from different TEs, as well as the advantages of the interleaved acquisition over the single-shot method at similar TEs.

RESULTS

The decreased distortion and blur from using a multishot acquisition can be noted in Fig. 3. Both three- and four-echo PERMEATE, and GRE-ssEPI were performed on a volunteer, and the slice at the MCA level is shown. Partial Fourier encoding was required in the single-shot scan in order to collect the two earliest TEs. Susceptibility gradients at this level from the auditory canal and the frontal sinuses cause well-known distortion and pile-up artifacts in the ssEPI images. These artifacts (most notably in the temporal lobes) are greatly reduced in the three- and fourshot PERMEATE images. The geometric distortion and short T_2^* from susceptibility gradients near the frontal sinuses leave little signal in the final echo near the MCAs. Do note that this final echo is normally the only one acquired in PWI studies.

Figure 4 summarizes raw images from four out of 15 slices acquired with a three-shot, three-echo PERMEATE sequence. Each image is a hybrid brain image, where the left side (subject's right hemisphere) shows one prebolus time point. The right side (subject's left hemisphere) shows the raw image acquired during the peak of the bolus passage. Current DSC methods acquire only the last echo, and the many areas of low signal in the prebolus volumes in this echo are problematic. The low image intensity reflects mostly the contribution of the additive Rician noise, rather than the tissue signal. The baseline image intensity used for single-echo ΔR_2^* calculations (Eq. [3]) has therefore been artificially set. The increased R_2^* during bolus passage is evident. During bolus passage, the tissue signal reduces, especially in areas near the large vessels, but the additive noise remains. The rectified noise at these locations artificially increases ΔT_2^* (therefore lowering ΔR_2^*), resulting in lowered estimation of contrast concentration, thereby hampering perfusion calculation. The inclusion of multiple, earlier echoes in the PERMEATE-weighted R_2^* fitting allows R_2^* mapping at areas where susceptibility artifacts precluded mapping in the single-echo approach, such as near sinuses or the auditory canals. Further, it removes most noise bias from low signal magnitude at these locations as well as near vessels during bolus passage.

Since the areas used to define the AIF have a quite short R_2^* during the bolus passage, the multiecho approach has distinct advantages here. Figure 5a shows the determined AIF from a three-interleaf, three-echo PERMEATE acquisition. The AIF was automatically determined using the resultant ΔR_2^* time course from the multiecho data, as well as by treating each of the three echoes as a separate dataset. On these single-echo datasets, $\Delta \tilde{R}_2^*$ from Eq. [3], rather than ΔR_2^* from Eq. [2], had to be used. The AIF is greatly underestimated by using the later single-echo data only, as the high concentration of contrast material reduces the MR magnitude signal so much that it bounces off the noise floor (25) during the peak due to the Rician noise distribution of magnitude data. Using the earliest echo gives a sharper and taller AIF curve, close to that of the multiecho fit. The multiecho fit gives the sharpest and tallest AIF, as it has removed any T_1 dependence. Figure 5b shows the ΔR_2^* contrast curves in gray matter (GM) and white matter (WM) tissue. The same dataset is used as for Fig. 5a, and the echoes are again also separated into single-echo datasets. The taller, dashed curves show a mean time course for an ROI taken in GM in the

frontal lobe, while the lower, dotted curves show the time course for an ROI in the WM at the same level. The lower tracer concentrations in the WM allow accurate mapping from any echo, or the multiecho fit. The higher concentrations found in the GM show underestimation during the bolus peak for the later echoes, though it is less drastic than that of the AIF. After the bolus has passed, residual tracer recirculation is evident. During this time, the multiecho fits show an increased tracer concentration as compared to the single-echo data. This is due to T_1-shortening effects induced by the remaining CA, resulting in higher tissue signal, which is interpreted as a lower apparent tracer concentration in the single-echo data. Sensitivity to T_1 increases with decreasing TR; however, shorter TRs are needed to achieve better temporal resolution. In PERMEATE, the multiple interleaves allowed 15 slices to be acquired in this TR, while multiple readouts removed the increased T_1 sensitivity. The shortest TE plot underestimates tracer concentration during this time more than the later echoes, as there is a smaller T_2^* weighting compared to later echoes, but equivalent, counteracting T_1 weighting.

The motion tolerance of this method is shown in Fig. 6. A three-interleaf, three-echo PERMEATE acquisition was performed clinically on a noncompliant patient. Imaging revealed an obvious frontal hemorrhage. The combined reconstruction of all three interleaves without PI acceleration is shown in Fig. 6a. Aside from having an unsuitably low temporal resolution, severe ghosting artifacts result due to patient motion. When each shot is reconstructed separately, a full image is formed, as shown in Fig. 6b–d. Image realignment is then performed to correct motion between the shots over all echoes based on estimates from the first echoes, since the motion between the echoes can be neglected.

Volunteer PWI hemodynamic parameters are shown in Fig. 7 for five of the 15 collected slices from a three-shot, three-echo PERMEATE acquisition. CBV, CBF, and MTT maps are shown in the first, second, and third rows, respectively. Good GM/WM contrast is evident in the CBF and CBV maps, while the MTT maps are characteristically flat except for the inherent GM/WM transit delay. Figure 8 shows the same scan protocol in a patient admitted for stroke-like symptoms. Though the CBV map appears normal, the CBF maps show several areas of decreased blood flow. Both CBF and MTT maps show an obvious hemispheric abnormality. In both the volunteer and patient maps, no geometric distortions or signal voids from susceptibility gradients are readily apparent. The major intracranial vessels can also be clearly delineated, which makes the selection of AIF candidate voxels much easier. The increased phase-encoding bandwidth reduced apparent vessel shifts during bolus passage, also aiding the shape of the determined AIF.

The resultant CBV and CBF values calculated in ROIs in the WM and GM for the volunteer data are presented in Table 1. As shown in Fig. 5, the underestimation of the AIF curve by the single-echo data, especially the latest echo, directly increases the calculated CBV. The underestimation of the tissue contrast is much smaller, and thus only slightly decreases the estimated CBV. The net result is a large overestimation of the CBV. As the CBF is directly inferred from the CBV, a concomitant increase in the CBF is also observable.

This phenomenon is also observable in the patient data. Hemodynamic maps from 25 patients acquired with the PERMEATE method, and 19 patients using single-echo GRE-

ssEPI were manually segmented into GM and WM ROIs in assumed healthy tissue that excluded obvious anatomic and/or perfusion abnormalities and vessels. The mean CBF and CBV values are summarized in Table 2. Values found in the PERMEATE scans agree well with values reported in the literature, and are obtained without the use of any corrective or normalizing factors. However, as most of this population had experienced some hemodynamic insult, comparison with reported values is somewhat impaired. Using the final echo only from these scans results in an increase in both CBF and CBV calculated values. The hemodynamic parameter values from this final echo are then close to the single-echo ssEPI values.

DISCUSSION

The use of autocalibrating PI with interleaved EPI has been shown to be useful for maintaining temporal resolution for a time-resolved study, such as PWI, while reducing artifacts related to ssEPI. This in turn will provide better fidelity and registration with other scans. The reduced readout train lengths also allowed the collection of multiple echoes without any scan time or slice coverage penalty. The use of multiple echoes had distinct advantages in this application as it allowed a more accurate estimate of the underlying concentration changes during bolus passage.

In this implementation, interleaved *M*-shot EPI trajectories are acquired rather than single-shot acquisitions. PI is calibrated from the low-temporal-resolution, fully sampled interleaved EPI volumes, and then used on each interleaf to restore the temporal resolution to that of a single-shot acquisition. That is, each interleaf is reconstructed independently to form a full, unaliased image. By controlling the data acquisition ordering, every temporally localized group of *M*shots may be combined to perform PI calibration without additional data collection. If desired, groups of interleaves may be reconstructed, thus reducing the reduction factor and increasing the SNR at the penalty of time resolution. For any reduction factor, the PI reconstruction kernel was calculated on the first echo of the first available volume, or combined volume, and applied to every echo in each acquisition across the entire time series. Finally, as several volumes exist before the bolus arrives, these volumes may be combined to make the hybrid-space GRAPPA weight estimation more numerically stable. This was found not to be necessary in this application as the least-square inversion was well overdetermined since the entire *k*-space, rather than only a center strip, could be used for the GRAPPA weight estimation. There was also no difference found when the weights determined from the early echo were applied to the other echo data sets. Using later echoes has the disadvantage of utilizing noisier data to estimate the weights.

A common problem in using CA concentration for the input function is that partial voluming of the tissue signal results in a complex and vessel orientation-dependent relationship between the concentration and the GRE signal (20). The higher phase-encoding bandwidth aids acquisition of inferior brain slices, capturing the larger vessels that exist at these locations. The lower frequency shift during the CA passage combined with the moderate resolution increase greatly increases the chances of acquiring voxels containing only a blood signal, which would allow the use of the whole-blood concentration calibration.

One advantage of a single-shot method is its tolerance to patient motion. A very short EPI readout (less than 50–100 ms) effectively eliminates motion artifacts. In contrast, in an interleaved EPI acquisition, patient motion between the shots causes well-known ghosting in the final image. In the method presented here, each shot is short enough so that essentially no motion occurs during the readout, though motion may exist between shots. Motion between echoes was deemed insignificant due to their short (~15–20 ms) spacing. As each shot is reconstructed independently, image registration may be performed between images using any of a number of well-described methods (18). The estimation of the GRAPPA kernel had little dependence on motion between interleaves. A detailed description of this behavior will be presented in a forthcoming manuscript. In our study, patient motion was noted in only five out of 44 patients scanned. In these cases, as each shot is reconstructed to a full image, automatic retrospective motion compensation was performed by minimizing the SoS differences between adjacent images. In only one out of 44 cases was PWI mapping after retrospective motion compensation not diagnostic. This was due to severe through-plane motion, which would have also confounded a single-shot method. While the hybrid-space GRAPPA reconstruction is tolerant to patient motion, sensitivity encoding (SENSE) (26) reconstructions were reported to suffer from significant aliasing artifacts when the extent of motion was large enough that no sensitivity information was available at image locations that did not contain signal during calibration. At the same magnitude of motion, we do not see significant reconstruction artifacts with our augmented GRAPPA reconstruction.

The use of PI reduced the echo train length to such an extent that several echoes could be collected. As maximal T_2^* contrast is obtained when TE is equal to T_2^*, it is imperative to collect an echo at this time. In DSC-PWI, the tissue T_2^* demands TEs from 40 to 60 ms, while vessel contrast is maximal at earlier TEs. In this interleaved method, readout trains required 10–15 ms, which allowed several echoes to be collected before the classic DSC TE near 60 ms. Both three- and four-echo sequences were used for PWI. By covering TEs up to the longest T_2^* time, areas with shorter T_2^*, such as near large vessels, could also be mapped for contrast changes. Through this method, EPI readout times could be shortened enough, while retaining resolution and increasing slice coverage, that more than two echoes could be acquired. This approach also allows the fitting process to avoid using echoes where the signal voids or the Rice-Nakagami noise distribution of magnitude data causes the MR signal to bounce off the noise floor. That is, rectified noise boosts the low signal areas, leading to inaccurate estimates of the concentration of the contrast material. These signal voids are commonly seen at the TEs used with PWI in areas of high CA concentration, such as in or near vessels. When multiple echoes are acquired, later echoes may be selectively weighted by their squared magnitude, preserving the ability to calculate true R_2^* even in these areas. The findings in this study have great significance, since by measuring the ΔR_2^* time course simultaneously at several TEs and performing a side-by-side comparison of the different time courses for the different TEs, it was clearly demonstrated how much error is introduced for AIF and GM signal time courses when TEs that are typically reported for DSC exams are used. These biases directly influence the determined CBV and CBF, resulting in an overestimation of both these values. Although this noise bias effect is not surprising for the AIF, it is somewhat startling that this effect can also be seen on late-echo

ΔR_2^* curves for GM. However, the magnitude of this bias effect does depend somewhat on the baseline SNR, and thus may be more pronounced through the use of PI.

As readout trains were shortened, the temporal sharpness of each echo also increased due to the reduced T_2^* decay over the readout window. Further, sufficient brain coverage could still be achieved in a short TR. Here a 1225-ms TR allowed the collection of 15 slices. As with regular EPI, larger brain coverage can be traded for decreased temporal resolution. Short TRs give high temporal resolution, allowing better mapping of the tracer dynamics. This is of particular relevance for catching subtle changes in the already rapidly changing tissue residue function. However, the shortened TR is increasingly sensitive to T_1 and can also introduce bias in the concentration estimation if normalized to the baseline signal. Classically, the concentration of the contrast media is estimated from the T_2^* shortening effect. With a T_2^*-weighted sequence and relatively short TR, the T_1-shortenening of the contrast material also leads to some signal increase that, at least to some extent, offsets the T_2^* decrease and as an overall effect leads to an underestimation of the contrast concentration present. Interestingly, the TR of this sequence is not much shorter than others reported in the literature (11,27), but it shows T_1 contamination even in GM. The data from our study clearly demonstrate that T_1 relaxation can considerably confound conventional DSC PWI methods when TRs are chosen too short. A still shorter TR in the PERMEATE approach might also aid proper AIF determination when using a PI reduction factor that less than the number of interleaves. Although slice coverage would suffer, the increased T_1 weighting from this shorter TR would not affect R_2^* measurement, in contrast to a single-echo case. T_1 effects are particularly marked in leaky vessels, which allow contrast extravasation. Here, the use of a multiecho sequence allowed true R_2^* maps to be calculated at each time point, removing the T_1 bias. This benefit was previously studied (13) with a dual-echo method. In a dual-echo method, R_2^* mapping may be impaired due to bias from low signal in certain locations in the later echo image, as previously discussed. Finally, by not relying on a prebolus R_2^* measurement, systematic errors in the R_2^* time course such as from patient motion during the long (>1 min) scan time were removed.

Signal intensity in short-TE GRE images may vary quadratically with TE when in the static dephasing regime (28). The characteristic time t_c, at which the well-known monoexponential decay dominates, depends on the field strength and the difference in magnetic susceptibility $\Delta\chi$. While the shortest TE (~15 ms) is longer than the t_c = 5.9 ms during bolus peak ($\Delta\chi = 1 \times 10^{-7}$) (29,30), this effect may be present at lower CA concentrations; however, this was not studied in the present work.

One drawback to the use of PI is a reduced SNR resulting from both the reduced sampling time and the *g*-factor noise amplification. While *g*-factor noise was not problematic in this study, especially when a reduction factor of 3 was used, the $(M - 1)/(M)$ fewer profiles sampled present an unavoidable SNR penalty. In Ref. 31, an error propagation analysis showed that the acquisition of multiple echoes helps recover some of the SNR lost to PI when calculating R_2^* maps, since the time gained from the PI acquisition is invested in sampling more data distributed over three or four echoes. The exact amount recovered depends on the tracer concentration and TEs (31). For a TE near 60 ms, the multiecho

approach becomes beneficial when T_2^* drops below 100 ms, and can result in a twofold SNR increase as T_2^* approaches 20 ms. T_2^* times below 40 ms are common in tissue during bolus passage, and are even shorter near major feeding vessels.

For DSC at field strengths of 3T and above, PI-driven EPI acquisitions such as PERMEATE become crucial to overcome distortions and blurring. Moreover, the reduced T_2^* at these field strengths also leads to shorter optimal TEs, requiring short readouts. The increased base SNR and B_1 behavior allows for higher reduction factors before the images suffer from *g*-factor-related noise (32). Taken together, these findings indicate that the optimum number of echoes in PERMEATE could remain constant while the latest TE and the readout length of each echo are reduced. This leads to an overall increase in slice coverage per unit of time.

CONCLUSIONS

An interleaved multiecho approach for DSC-PWI combined with *k*-space-based PI reconstruction of individual interleaves has been presented and implemented for clinical perfusion imaging. This method provides distortion and blur reduction over conventional T_2^*-weighted ssEPI. Further, multiple echoes could be acquired to remove T_1 bias as well as to allow R_2^* mapping in locations that were previously difficult to measure due to noise bias of the low signal magnitude, such as near the highly saturated feeding vessels or areas of large susceptibility gradients. Satisfying coverage (15 slices) could be acquired with three or four echoes, with an effective temporal resolution of only 1.225 s (producing 2200–2900 images per minute). This temporal resolution is higher than that used in most previous works, and allows excellent characterization of the rapid hemodynamic changes. The autocalibration approach also reduced the motion sensitivity of the sequence, which can be otherwise problematic in stroke patients. Despite the SNR reduction introduced by PI, the overall SNR of the quantification was not excessively compromised because quasi-continuous measurements were taken over three to four echoes for each time point and each slice. A three-interleaf, three-echo sequence offered the best trade-off between reduced image distortions and blur, yet with enough SNR and motion robustness to be used clinically in stroke patients. Certainly, DSC-PWI still suffers from a few other shortcomings that have not been addressed in this work, such as the orientation of the vessel relative to B_0, the different concentration sensitivity of large vessels and capillaries due to various amounts of static and dynamic dephasing components (29,30,33), and the global AIF model. However, providing a pulse sequence that offers significantly diminished EPI-related distortions and is less sensitive to signal saturation effects and T_1 contamination is a logical next step towards improved, quantitative perfusion MRI.

Acknowledgments

Grant sponsor: Lucas Foundation; Grant sponsor: Oak Foundation; Grant sponsor: National Institutes of Health; Grant number: 1R01EB002771; Grant sponsor: Center of Advanced MR Technology at Stanford; Grant number: P41RR09784.

REFERENCES

1. Rose SE, Janke AL, Griffin M, Strudwick M, Finnigan S, Semple J, Chalk JB. Improving the prediction of final infarct size in acute stroke with bolus delay-corrected perfusion MRI measures. J Magn Reson Imaging. 2004; 20:941–947. [PubMed: 15558572]
2. Rosen BR, Belliveau JW, Buchbinder BR, McKinstry RC, Porkka LM, Kennedy DN, Neuder MS, Fisel CR, Aronen HJ, Kwong KK, Weisskoff RM, Cohen MS. Contrast agents and cerebral hemodynamics. Magn Reson Med. 1991; 19:285–292. [PubMed: 1881317]
3. Rempp KA, Brix G, Wenz F, Becker CR, Guckel F, Lorenz WJ. Quantification of regional cerebral blood flow and volume with dynamic susceptibility contrast-enhanced MR imaging. Radiology. 1994; 93:637–641. [PubMed: 7972800]
4. Guckel F, Brix G, Rempp K, Deimling M, Rother J, Georgi M. Assessment of cerebral blood volume with dynamic susceptibility contrast enhanced gradient-echo imaging. J Comput Assist Tomogr. 1994; 18:344–351. [PubMed: 8188897]
5. Østergaard L, Weisskoff RM, Chesler DA, Gyldensted C, Rosen BR. High resolution measurement of cerebral blood flow using intravascular tracer bolus passages. Part I: Mathematical approach and statistical analysis. Magn Reson Med. 1996; 36:715–725. [PubMed: 8916022]
6. Mansfield P. Multi-planar image-formation using NMR spin echoes. J Phys C Solid State. 1977; 10:L55–L58.
7. Constable RT, Gore JC. The loss of small objects in variable TE imaging: implications for FSE, RARE, and EPI. Magn Reson Med. 1992; 28:9–24. [PubMed: 1435225]
8. Farzaneh F, Riederer SJ, Pelc NJ. Analysis of T2 limitations and off-resonance effects on spatial resolution and artifacts in echo-planar imaging. Magn Reson Med. 1992; 14:123–139. [PubMed: 2352469]
9. Ellinger R, Kremser C, Schocke MF, Michael FH, Kolbitsch C, Griebel J, Felber SR, Aichner FT. The impact of peak saturation of the arterial input function on quantitative evaluation of dynamic susceptibility contrast-enhanced MR studies. J Comput Assist Tomogr. 2000; 24:942–948. [PubMed: 11105716]
10. Bammer R, Keeling SL, Augustin A, Pruessmann KP, Wolf R, Stollberger R, Hartung V, Fazekas F. Improved diffusion-weighted single-shot echo-planar imaging (EPI) in stroke using sensitivity encoding (SENSE). Magn Reson Med. 2001; 46:548–554. [PubMed: 11550248]
11. Stollberger R, Fazekas F. Improved perfusion and tracer kinetic imaging using parallel imaging. Top Magn Reson Imaging. 2004; 15:245–255. [PubMed: 15548955]
12. Griswold MA, Jakob PM, Chen Q, Goldfarb JW, Manning WJ, Edelman RR, Sodickson DK. Resolution enhancement in single-shot imaging using simultaneous acquisition of spatial harmonics (SMASH). Magn Reson Med. 1999; 41:1236–1245. [PubMed: 10371457]
13. Vonken EP, van Osch MJ, Bakker CJ, Viergever MA. Simultaneous quantitative cerebral perfusion and Gd-DTPA extravasation measurement with dual-echo dynamic susceptibility contrast MRI. Magn Reson Med. 2000; 43:820–827. [PubMed: 10861876]
14. Vonken EJ, van Osch MJ, Bakker CJ. Measurement of cerebral perfusion with dual-echo multi-slice quantitative dynamic susceptibility contrast MRI. J Magn Reson Imaging. 1999; 10:109–117. [PubMed: 10441012]
15. Newbould, R.; Skare, S.; Clayton, DB.; Alley, MT.; Albers, G.; Lansberg, M.; Bammer, R. PERMEATE: High temporal resolution multi-echo/multislice dynamic susceptibility contrast perfusion imaging using GRAPPA EPI. Proceedings of the 14th Annual Meeting of ISMRM; Seattle, WA, USA. 2006. (Abstract 673).
16. Skare, S.; Bammer, R. Spatial modeling of GRAPPA weights. Proceedings of the 13th Annual Meeting of ISMRM; Miami Beach, FL, USA. 2005. (Abstract 2422).
17. Skare S, Newbould RD, Clayton DB, Bammer R. Propeller EPI in the other direction. Magn Reson Med. 2006; 55:1298–1307. [PubMed: 16676335]
18. Friston KJ, Ashburner J, Frith CD, Poline J-B, Heather JD, Frackowiak. Spatial registration and normalization of images. Hum Brain Mapp. 1995; 3:165–189.

19. Mlynash M, Eyngorn I, Bammer R, Moseley M, Tong DC. Automated method for generating the arterial input function on perfusion-weighted MR imaging: validation in patients with stroke. AJNR Am J Neuroradiol. 2005; 26:1479–1486. [PubMed: 15956519]
20. van Osch M, Vonken E, Viergever M, van der Grond J, Bakker C. Measuring the arterial input function with gradient echo sequences. Magn Reson Med. 2003; 49:1067–1076. [PubMed: 12768585]
21. Kjølby BF, Østergaard L, Kiselev VG. Theoretical model of intravascular paramagnetic tracers' effect on tissue relaxation. Magn Reson Med. 2006; 56:187–197. [PubMed: 16724299]
22. Wu O, Østergaard L, Weisskoff RM, Benner T, Rosen BR, Sorensen AG. Tracer arrival timing-insensitive technique for estimating flow in MR perfusion-weighted imaging using singular value decomposition with a block-circulant deconvolution matrix. Magn Reson Med. 2003; 50:164–174. [PubMed: 12815691]
23. Meier P, Zierler LL. On the theory of the indicator-dilution method for measurement of blood flow and volume. J Appl Physiol. 1954; 6:731–744. [PubMed: 13174454]
24. Zierler KL. Theoretical basis of indicator-dilution methods for measuring flow and volume. Circ Res. 1962; 10:393–407.
25. Sijbers J, den Dekker AJ, Audekerke JV, Verhoye M, Dyck DV. Estimation of the noise in magnitude MR images. Magn Reson Imaging. 1998; 16:87–90. [PubMed: 9436952]
26. Pruessmann KP, Weiger M, Scheidegger MB, Boesiger P. Sensitivity encoding for fast MRI. Magn Reson Med. 1999; 42:952–962. [PubMed: 10542355]
27. Simonsen CZ, Østergaard L, Smith DF, Vestergaard-Poulsen P, Gyldensted C. Comparison of gradient- and spin-echo imaging: CBF, CBV, and MTT measurements by bolus tracking. J Magn Reson Imaging. 2000; 12:411–416. [PubMed: 10992308]
29. Weisskoff RM, Zuo CS, Boxerman JL, Rosen BP. Microscopic susceptibility variation and transverse relaxation: theory and experiment. Magn Reson Med. 1994; 31:601–610. [PubMed: 8057812]
30. Boxerman JL, Hamberg LM, Rosen BR, Weisskoff RM. MR contrast due to intravascular magnetic susceptibility perturbations. Magn Reson Med. 1995; 34:555–566. [PubMed: 8524024]
31. Jochimsen TH, Newbould RD, Skare ST, Clayton DB, Albers GW, Moseley ME, Bammer R. Identifying systematic errors in quantitative dynamic-susceptibility contrast perfusion imaging by high resolution multiecho parallel EPI. NMR Biomed. (in press).
32. Wiesinger F, Van de Moortele PF, Adriany G, Zanche ND, Ugurbil K, Pruessmann KP. Potential and feasibility of parallel MRI at high field. NMR Biomed. 2006; 19:368–378. [PubMed: 16705638]
33. Kiselev VG. On the theoretical basis of perfusion measurements by dynamic susceptibility contrast MRI. Magn Reson Med. 2001; 46:1113–1122. [PubMed: 11746577]

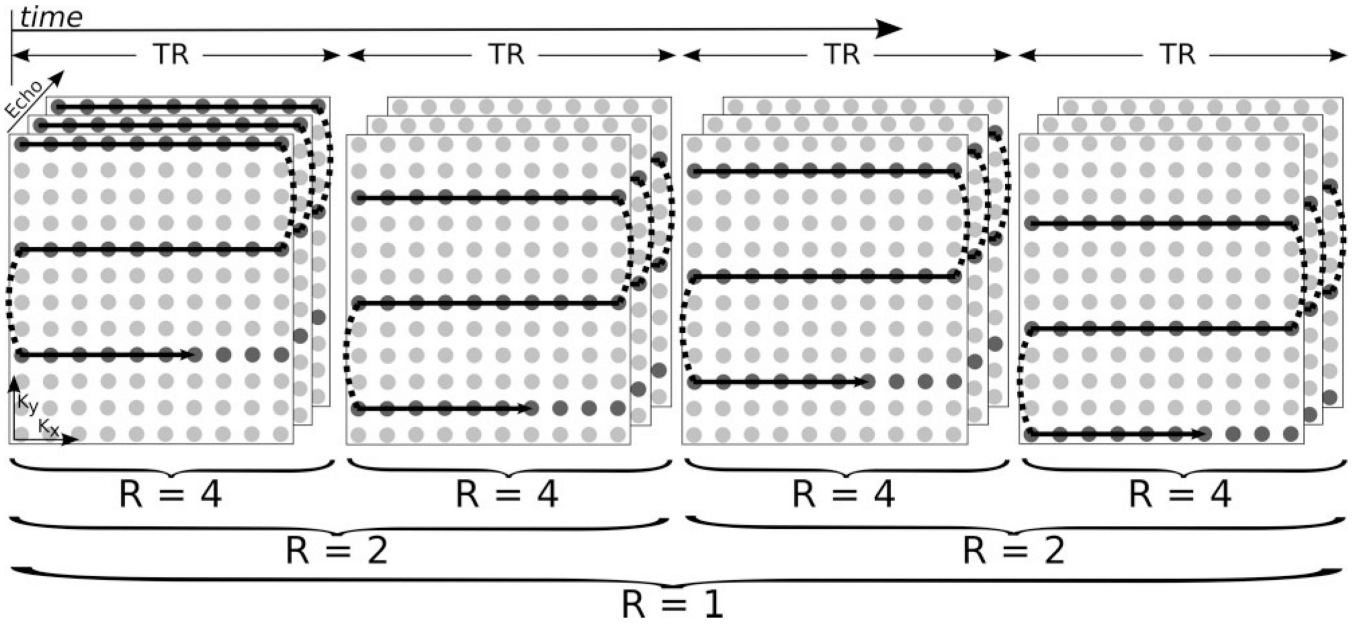

FIG. 1.

k-Space acquisition pattern for the first four time points in a four-shot dynamic series with three echoes. Only a single slice is shown for clarity. Data are acquired in an interleaved fashion, and the combination of four subsequent interleaves yields a fully sampled *k*-space (*R* = 1) from which coil sensitivity maps or GRAPPA weights can be determined. Maximum temporal resolution (Δt = TR) can be achieved with *R* equal to the number of interleaves (here, 4). A reduced temporal resolution with increased SNR is possible with this acquisition pattern, as interleaving results in *R* = 2 by combining pairs of shots, or *R* = 1 by combining all four shots.

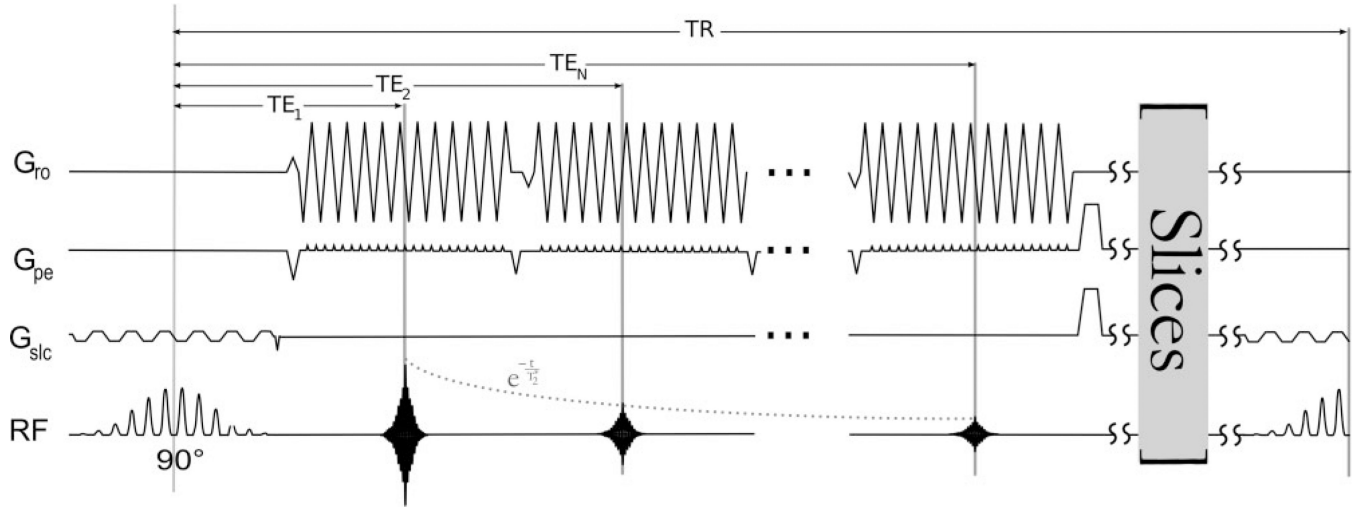

FIG. 2.

An *N*-echo PERMEATE acquisition. A spatial-spectral excitation is followed by *N* interleaved EPI readouts, each of which acquires the same 1/*M*th of a fully interleaved *k*-space. Prephasing and rephasing *y*-gradients are combined for time savings. Gradient spoilers end the acquisition, and slice interleaving fills the TR interval. After every *M* TR interval a complete *k*-space is formed for PI calibration, and the subsequent hybrid-space GRAPPA reconstruction of each individual interleaf restores the temporal resolution of each echo back to a single TR.

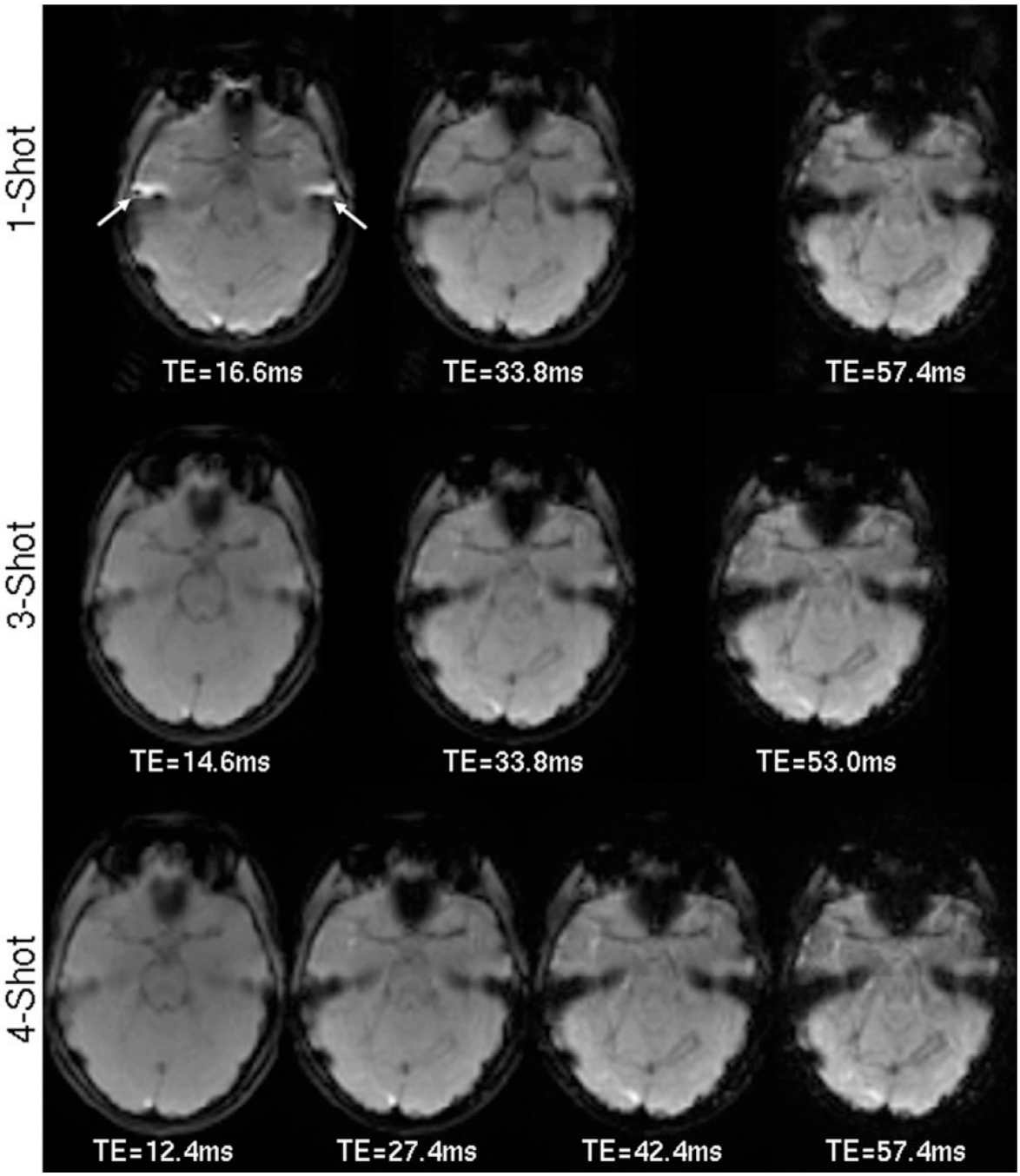

FIG. 3.

Distortion reduction from a PERMEATE-style acquisition. The top row shows the current standard single-echo GRE ssEPI taken at three TEs approximately equal to those in the three-shot, three-echo and four-shot, four-echo PERMEATE acquisitions in the middle and bottom rows, respectively. TEs are not exact due to the longer readout with GRE-ssEPI. Reduced distortions near the auditory canals (arrows) are most notable. Current DSC methods only acquire the final echo, where susceptibility gradients have eroded much of the signal, even encroaching near the MCAs, which are commonly used to determine the AIF.

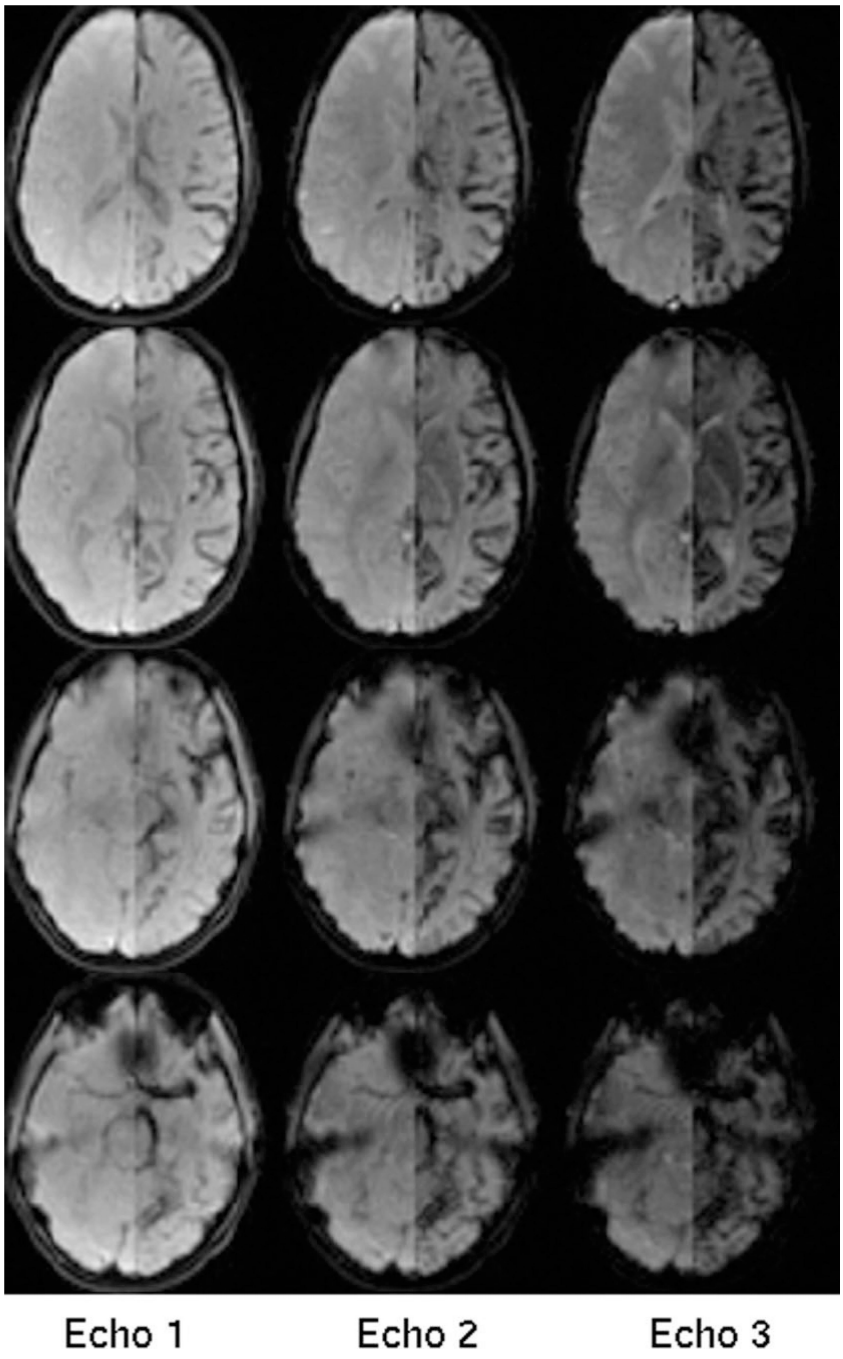

FIG. 4.

Raw images for four of 15 slices from a three-shot, three-echo PERMEATE acquisition. The left hemisphere (subject's right) shows a prebolus volume, whereas the right hemisphere reflects the signal level during bolus peak. Current DSC methods acquire only the last echo shown. The many areas of low signal in this echo are problematic for R_2^* estimation and hamper perfusion calculation at these locations. The inclusion of multiple echoes in the PERMEATE approach allows for improved R_2^* mapping, especially at these locations.

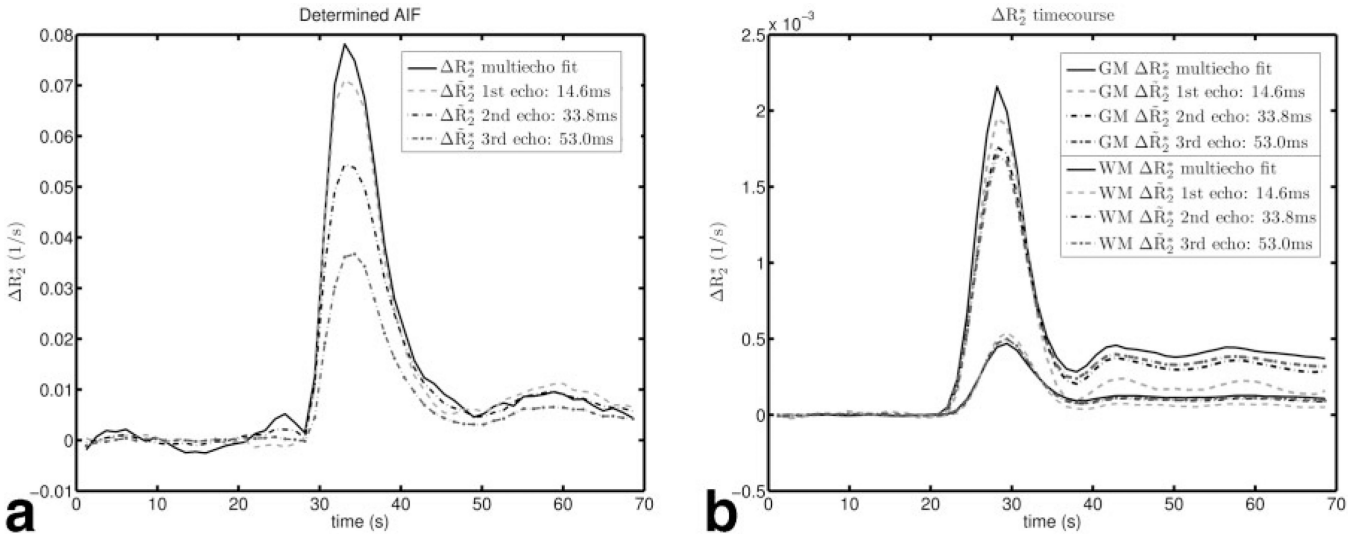

FIG. 5.

Single-echo underestimation of ΔR_2^* time courses. A three-interleaf, three-echo PERMEATE acquisition was performed on a normal volunteer. PERMEATE multiecho perfusion calculations were performed using direct R_2^* calculation. Each echo was additionally treated as a separate, single-echo acquisition. ΔR_2^* time courses are shown using Eq. [2] PERMEATE data, or Eq. [3] in pseudo-single-echo sets. The third-echo-only time course mimics a standard GRE-EPI DSC experiment. **a:** The AIF determined for each dataset is shown. Later echoes underestimate the size of the AIF due to noise bias as the signal saturates during the bolus maximum. **b:** The R_2^* tissue time courses in GM and WM are plotted. The increased concentration of the tracer in GM shows underestimation by the later, single-echo datasets, while WM is estimated well by all methods. After bolus passage, T_1 shortening underestimates the tracer concentration in the single-echo datasets due to the short TR used to maintain high temporal resolution. This effect is most notable in the early, single echo, which has less T_2^* weighting but equal T_1 weighting compared to the later echoes.

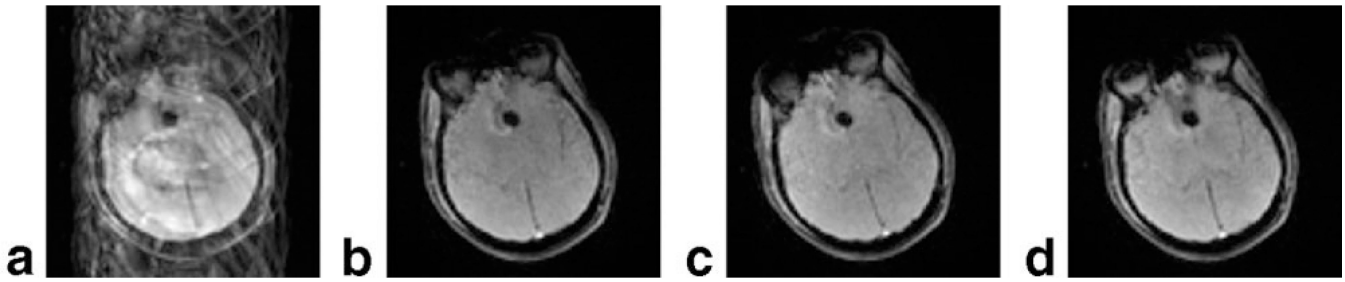

FIG. 6.

Motion tolerance in a three-shot, three-echo PERMEATE acquisition. In this clinical patient with obvious frontal hemorrhage (arrow), severe patient motion combined with a classic interleaved EPI acquisition (**a**) results in major residual ghosting artifacts. In the PERMEATE approach, each shot is reconstructed separately. Here, each of the three shots from (**a**) are reconstructed separately as (**b–d**). These ghost-free images may then be coregistered. In practice, motion correction parameters from the first echo are applied to each subsequent echo, which assumes negligible motion in the short time between the echoes. Only the first echo is shown in this figure for brevity.

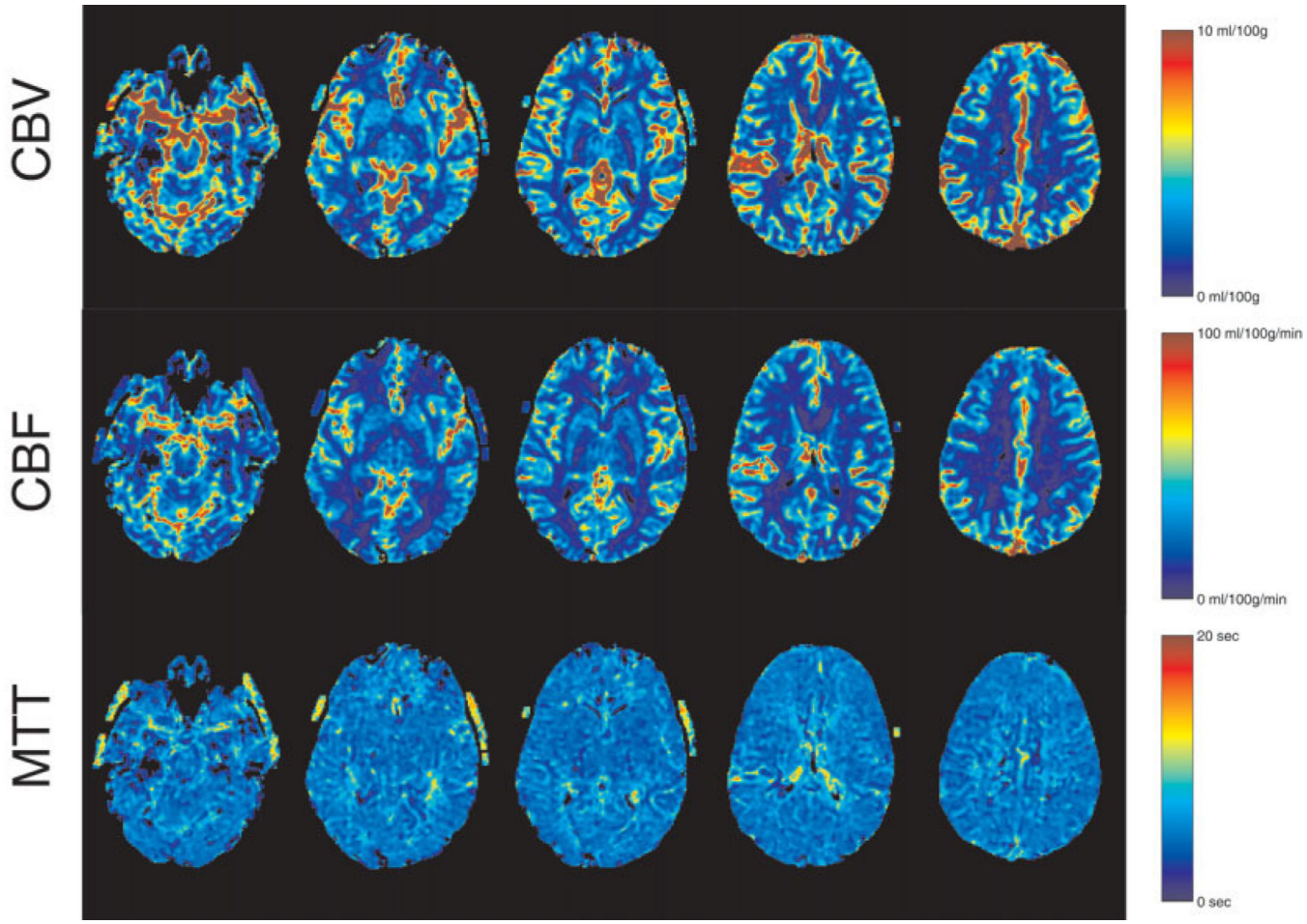

FIG. 7.

Hemodynamic maps from a healthy volunteer, using the three-shot, three-echo PERMEATE approach with $R = 3$. Sixty volumes of 15 three-echo, 5-mm slices were obtained using a temporal resolution of 1.225 s. Good GM/WM contrast is apparent in the CBF and CBV maps, and the MTT maps show no areas of greatly increased transit time.

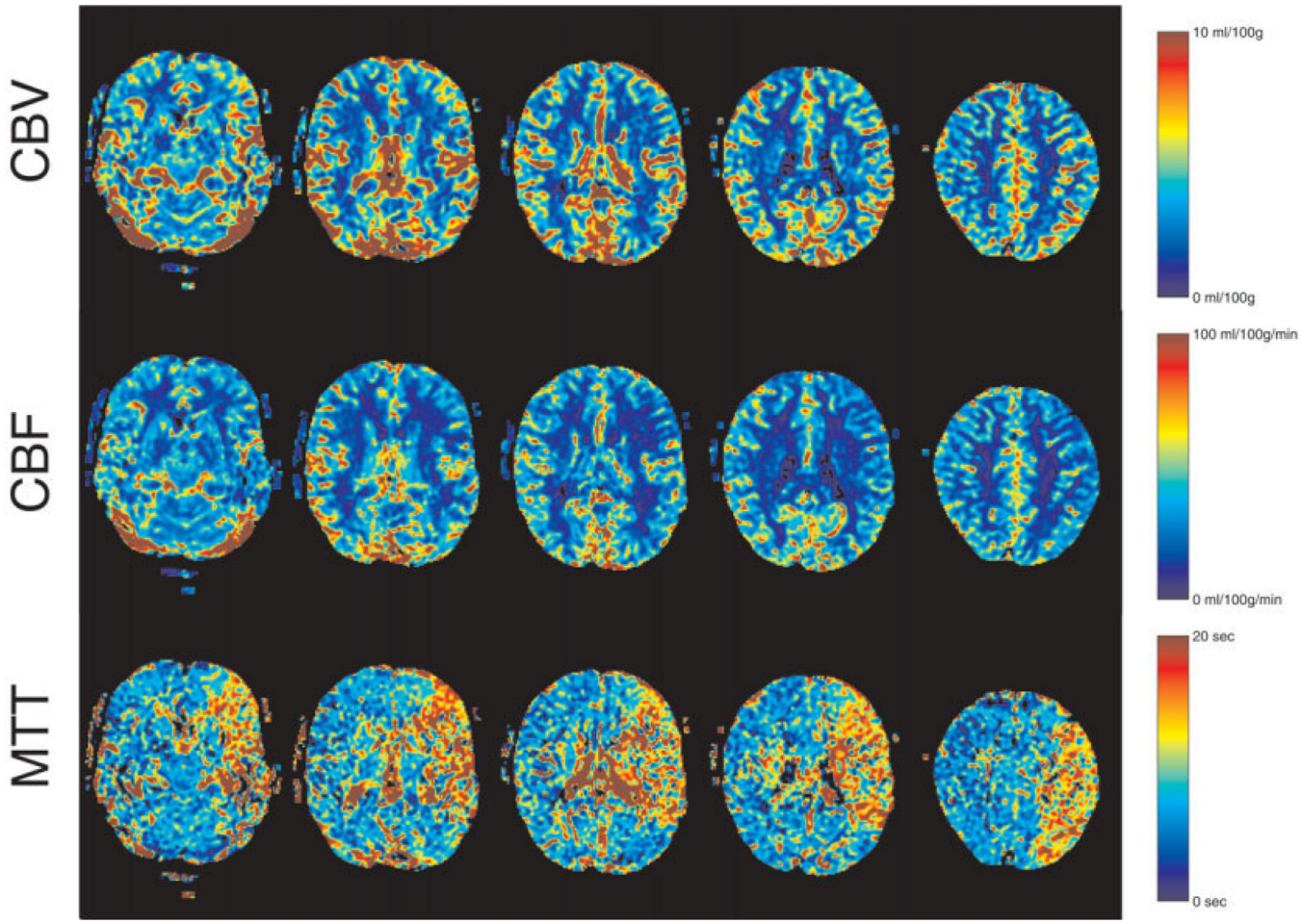

FIG. 8.

Hemodynamic maps from a 62-year-old male admitted for headaches and right-sided weakness, calculated using a PERMEATE scan identical to that shown in Fig. 8. Significantly reduced blood flow can be seen in the vascular territory of the left MCA. Corresponding diffusion imaging revealed several focal lesions, while PWI revealed a large left hemispherical defect. The diagnosis was an ICA occlusion from vessel dissection.

Table 1

CBF and CBV Overestimation From Single- and Multiple-Echo Perfusion Mapping

	All echoes	First echo	Second echo	Third echo
CBF (ml/100 g/min)				
GM	52.61 ± 5.30	129.41 ± 11.07	74.06 ± 7.25	80.38 ± 6.37
WM	18.67 ± 3.26	36.13 ± 4.00	20.80 ± 3.45	27.56 ± 3.95
CBV (ml/100 g)				
GM	5.06 ± 1.85	11.97 ± 3.67	7.64 ± 2.75	8.97 ± 2.59
WM	1.68 ± 0.94	2.71 ± 1.18	1.90 ± 0.96	2.76 ± 1.18

Table 2

CBF and CBV Estimation by PERMEATE in 25 Patients and Single-Echo GRE-ssEPI in 19 Patients

	PERMEATE	PERMEATE, last echo only	GRE-ssEPI
CBF (ml/100 g/min)			
GM	36.85 ± 4.61	57.81 ± 5.82	55.36 ± 6.59
WM	16.57 ± 2.78	24.58 ± 3.65	22.28 ± 3.86
CBV (ml/100 g)			
GM	5.07 ± 1.63	8.08 ± 2.67	7.77 ± 2.07
WM	2.13 ± 1.04	3.13 ± 1.55	2.98 ± 1.24